Available online at www.sciencedirect.com
SCIENCE DIRECT
Journal of the European Ceramic Society 26 (2006) 909–914
www.elsevier.com/locate/jeurceramsoc

Structural and electrical properties of $FeMg_{0.7}Cr_{0.6}Co_{0.7-x}Al_xO_4$ ($0 \leq x \leq 0.3$) thick film NTC thermistors

K. Park *

Department of Advanced Materials Engineering, Center for Advanced Materials, Sejong University, Seoul 143-747, Republic of Korea

Received 27 September 2004; accepted 10 December 2004
Available online 21 February 2005

Abstract

The microstructure and electrical properties of $FeMg_{0.7}Cr_{0.6}Co_{0.7-x}Al_xO_4$ ($x = 0$, 0.1, 0.2, and 0.3) thick film negative temperature coefficient (NTC) thermistors, fabricated by screen printing, were studied. The sintered $FeMg_{0.7}Cr_{0.6}Co_{0.7-x}Al_xO_4$ bodies were the solid solutions of the constituent oxides along with a small amount of $MgAl_2O_4$. The electrical resistivity increased with sintering temperature mainly because of an increase in the amount of insulating $MgAl_2O_4$ resulting from the partial decomposition of the solid solutions during sintering. In addition, the added Al_2O_3 led to a significant increase in the resistivity. The effect of the sintering temperature and Al_2O_3 on the electrical properties of the NTC thermistors was discussed.

Keywords: $Fe(Mg,Cr,Co,Al)_2O_4$; Thermistors; Al_2O_3; Electrical properties; Microstructure

1. Introduction

Transition metal oxides were first reported for use as thermally sensitive resistors in 1979 by Macklen.[1] Since their resistivity decreases exponentially with temperature, they are referred to as negative temperature coefficient (NTC) thermistors, which are semiconducting polycrystalline ceramics. The NTC thermistor ceramics are sintered typically at 1100–1400 °C, depending on the composition. In general, the sintering and cooling atmospheres are air and, as a result, the ceramics oxidize during cooling down. The high temperature sensitivity of the resistivity allows it to be used in many applications, including temperature measurements and regulations, temperature drift compensation, voltage regulation, fluid flow rate measurements, etc.[1]

Traditionally, most of the NTC thermistors used in practice are based on solid solutions of transition metal oxides with the spinel structure of the general formula AB_2O_4.[2–5] In the spinel structure, there are two sites available for the cations, i.e., the tetrahedral site, the A-site, and the octahedral site, the B-site. In particular, a high level of technological reproducibility can be achieved in the Mn–Cu–Co, Mn–Co–Ni, and Mn–Cu–Ni oxide systems.[6] The composition of the thermistors strongly affects the distribution of cations and thus changes the physical properties.[7–12]

The apparent low mobility of charge carriers and the electrical conduction phenomena in the NTC thermistors are not adequately interpreted by the ordinary band theory of semiconduction and are poorly understood. Several models invoke the small polaron theory, known as a "hopping" mechanism, which is associated with a phonon-assisted jump of carriers between cations of differing oxidation states on the octahedral sites of the spinel structure.[13–19] For example, in the nickel manganites, electrical conduction is due to an electron jump between the Mn^{4+} and Mn^{3+} cations present on the octahedral sites.[20] The octahedral cations in the spinel structure lie in chains along some <1 1 0> directions. These vectors represent the smallest intercationic distances within the unit cell.[2]

* Tel.: +82 2 3408 3777; fax: +82 2 3408 3664.
E-mail address: kspark@sejong.ac.kr.

0955-2219/$ – see front matter © 2005 Elsevier Ltd. All rights reserved.
doi:10.1016/j.jeurceramsoc.2004.12.021

Manganites have attracted special attention due to their low room-temperature resistivity and are thus used extensively for low-temperature thermistors below 300 °C.[7,21–24] It is necessary to develop the composition for industrial and domestic applications in a wide temperature range. Many workers have extensively studied the electrical properties of $Sr_7Mn_4O_{15}$, $LaTi^{IV}_yCo^{II}_yCo^{III}_{1-2y}O_3$, $NiO–Mn_3O_4–Fe_2O_3$, $TiO_2–Al_2O_3–Y_2O_3$, and $CoO–Al_2O_3$ systems for applications at higher temperatures.[25–28] The $Sr_7Mn_4O_{15}$ with a K_2NiF_4 type structure is difficult for reproducible preparation and therefore less suitable for industrial production.[25] The $LaTi^{IV}_yCo^{II}_yCo^{III}_{1-2y}O_3$, based on the perovskite type structure, for temperature measurements is not suitable due to an insufficient sensitivity.[26] Furthermore, although the concepts of thick film NTC devices are quite attractive from a system design and manufacturing viewpoint, they are not widely known and used. Thick film devices are useful to accommodate the demands of miniaturization, circuit complexity, or multilayer assembles.[29,30] It is thus required to extend the selection of suitable compositions with the desired electrical properties and the concept of system designs for high temperature applications. In the present study, the microstructure and electrical properties of the $FeMg_{0.7}Cr_{0.6}Co_{0.7-x}Al_xO_4$ ($x = 0$, 0.1, 0.2, and 0.3) thick film NTC thermistors fabricated by screen printing were studied, especially with regard to the partial substitution of Al for Co in the $FeMg_{0.7}Cr_{0.6}Co_{0.7-x}Al_xO_4$ thermistors.

2. Experimental

To achieve a high level of local homogeneity in the microstructure and reproducible electrical characteristics, great attention has been paid to the purity and the morphology of the used oxides. High-purity Fe_2O_3, MgO, Cr_2O_3, Co_3O_4, and Al_2O_3 powders (Kojundo Chemical Lab Co., Japan) were used in this study. A set of $FeMg_{0.7}Cr_{0.6}Co_{0.7-x}Al_xO_4$ ($x = 0$, 0.1, 0.2, and 0.3) thick film NTC thermistors were prepared by screen printing. Fe_2O_3, MgO, Cr_2O_3, Co_3O_4, and Al_2O_3 powders were weighed in appropriate proportions. The mixture of weighed powders and ethyl alcohol was ball-milled for 24 h in a teflon jar using ZrO_2 as the grinding media. The ball-milled slurries were dried at 80 °C in an oven for 24 h. Subsequently, a thixotropic paste was formulated by mixing the dried powder (40 wt.%) with a vehicle (60 wt.%), composed of a resin (ethyl cellulose) and an organic solvent (n-butyl carbitol acetate and α-terpineol).

The thermistor pastes of ∼15 μm thickness were printed on the Al_2O_3 substrate of 8.0 mm × 9.0 mm × 0.38 mm with a manual thick film printer (Han Sung Systems, Model: HSP-12A) equipped with a 200 mesh screen. The screen is an essential tool determining the thickness of the printed films. The paste was pressed through the screen onto the substrate by applying a printer stroke with a squeeze blade. After the samples were dried at 80 °C for 10 min, they were sintered at 1300–1400 °C for 4 h. The Pt pastes of ∼15 μm thickness were coated on the sintered ceramic films and Al_2O_3 substrate

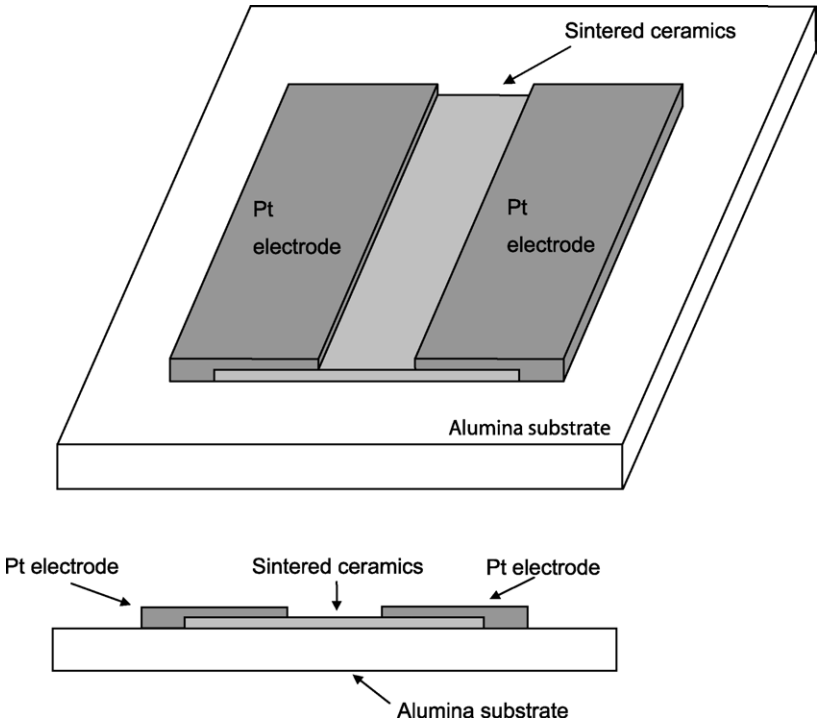

Fig. 1. Schematic diagram of the $FeMg_{0.7}Cr_{0.6}Co_{0.7-x}Al_xO_4$ ($x = 0$, 0.1, 0.2, and 0.3) thick film NTC thermistors prepared in this study.

by screen printing in order to enable electrical measurements to be made through the thick films. After the Pt pastes were dried at room temperature, the samples were heated at 800 °C for 10 min. The schematic structure of the NTC thick film thermistors prepared in this study is represented in Fig. 1.

The crystalline structure and the morphology of the thick film ceramics were investigated by X-ray diffraction (XRD) and scanning electron microscopy (SEM), respectively. The thicknesses of the thick films and Pt electrodes were measured from cross-sectional analysis of the fractured samples, using SEM. The average grain size of the ceramics was estimated by the line-intersecting method. The samples were held with a holder in a quartz tube furnace, and their temperatures were measured with a digital thermometer. The electrical resistance of the samples in the furnace was measured with a digital multi-meter from 200 °C up to 340 °C in steps of 10 °C.

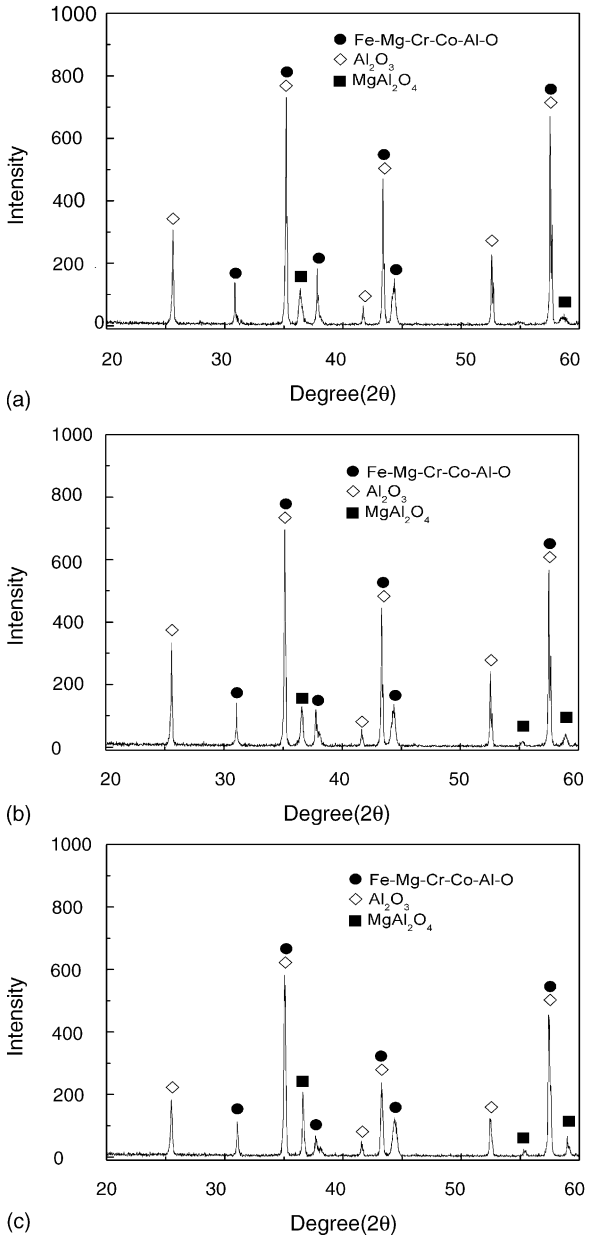

Fig. 2. XRD patterns from the $FeMg_{0.7}Cr_{0.6}Co_{0.5}Al_{0.2}O_4$ thick films sintered at (a) 1300 °C, (b) 1350 °C, and (c) 1400 °C.

3. Results and discussion

The $FeMg_{0.7}Cr_{0.6}Co_{0.7-x}Al_xO_4$ ($x = 0$, 0.1, 0.2, and 0.3) thick films contained the solid solutions of Fe–Mg–Cr–Co–(Al) oxides with a cubic spinel structure and a small amount of $MgAl_2O_4$ with a cubic spinel structure ($a = 8.0831$ Å). The $MgAl_2O_4$ in the thick films was likely to be formed by the partial decomposition of the solid solutions during sintering. The amount of $MgAl_2O_4$ increased with increasing sintering temperature. For example, XRD patterns

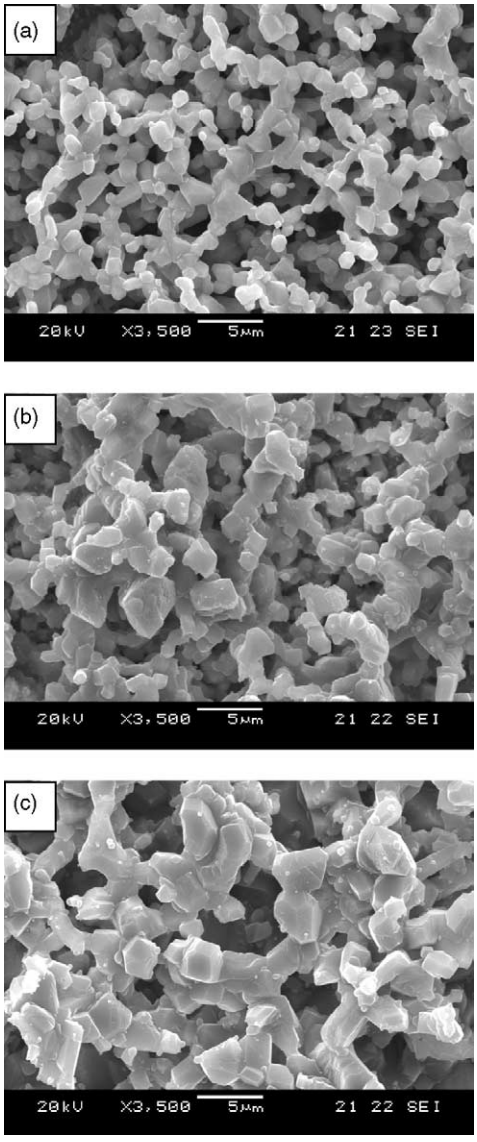

Fig. 3. SEM images obtained from the surface of the $FeMg_{0.7}Cr_{0.6}Co_{0.6}Al_{0.1}O_4$ thick films sintered at (a) 1300 °C, (b) 1350 °C, and (c) 1400 °C.

from the sintered bodies of $FeMg_{0.7}Cr_{0.6}Co_{0.5}Al_{0.2}O_4$ are shown in Fig. 2. The peaks corresponding to Al_2O_3 originate from the substrate.

Fig. 3 shows the SEM images obtained from the surface of the $FeMg_{0.7}Cr_{0.6}Co_{0.6}Al_{0.1}O_4$ thick films sintered at 1300–1400 °C. The sintered bodies are porous, compared to the bulk samples with the same composition as these samples.[31] This is due to the low pressure during the screen printing and the evolution of organic binders in the paste during the sintering. As expected, the grain size of the sintered bodies increased with increasing sintering temperature. Fig. 4 represents the cross-sectional SEM image showing the $FeMg_{0.7}Cr_{0.6}Co_{0.5}Al_{0.2}O_4$ thick films and the Al_2O_3 substrate sintered at 1350 °C. The thick films printed on the Al_2O_3 substrate were highly homogeneous and adhered very well to the substrate.

Fig. 5 shows plots of the logarithms of the electrical resistivity, $\log \rho$, against the reciprocal of the absolute temperature, $1/T$, for the $FeMg_{0.7}Cr_{0.6}Co_{0.7-x}Al_xO_4$ ($x = 0$, 0.1, 0.2, and 0.3) thick film NTC thermistors sintered at various temperatures. It was found that the NTC thermistors operate steadily with the straight line relationship between these parameters over a wide temperature range, indicating NTC thermistor characteristics. The slope of the $\log \rho$ versus $1/T$ curve is taken generally as a measure of the activation energy of conductivity. The resistivity ρ can be expressed by the following Arrhenius equation:[1]

$$\rho = \rho_0 \exp\left(\frac{B}{T}\right) \quad (1)$$

where ρ_0 is the resistivity of the material at infinite temperature, T is the absolute temperature, and B is the B constant, sometimes called the coefficient of temperature sensitivity. In fact, the B constant has the dimensions of the absolute temperature and is given by

$$B = \frac{q}{k} \quad (2)$$

where q is the activation energy for electrical conduction and k is the Boltzmann constant. The activation energy is primarily the energy for the hopping process from a cation M^{n+} to $M^{(n+1)+}$ on the octahedral sites and, hence, for the mobility of the cations.[13–19] It is clear that the resistivity of all the samples followed basically the same thermally activated behavior represented by Eq. (1).

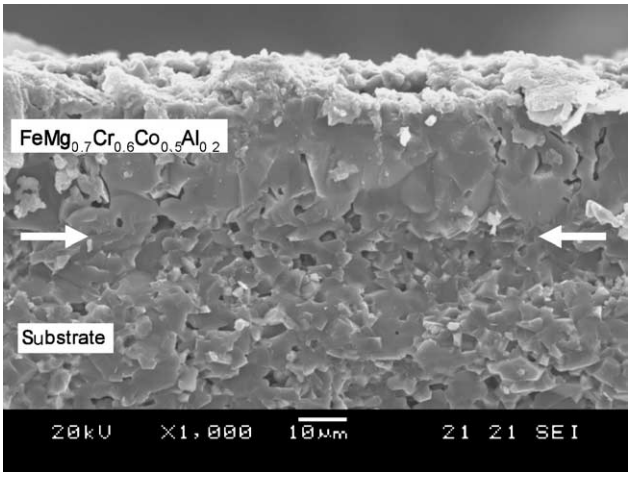

Fig. 4. Cross-sectional SEM image showing the $FeMg_{0.7}Cr_{0.6}Co_{0.5}Al_{0.2}O_4$ thick films and the Al_2O_3 substrate sintered at 1350 °C.

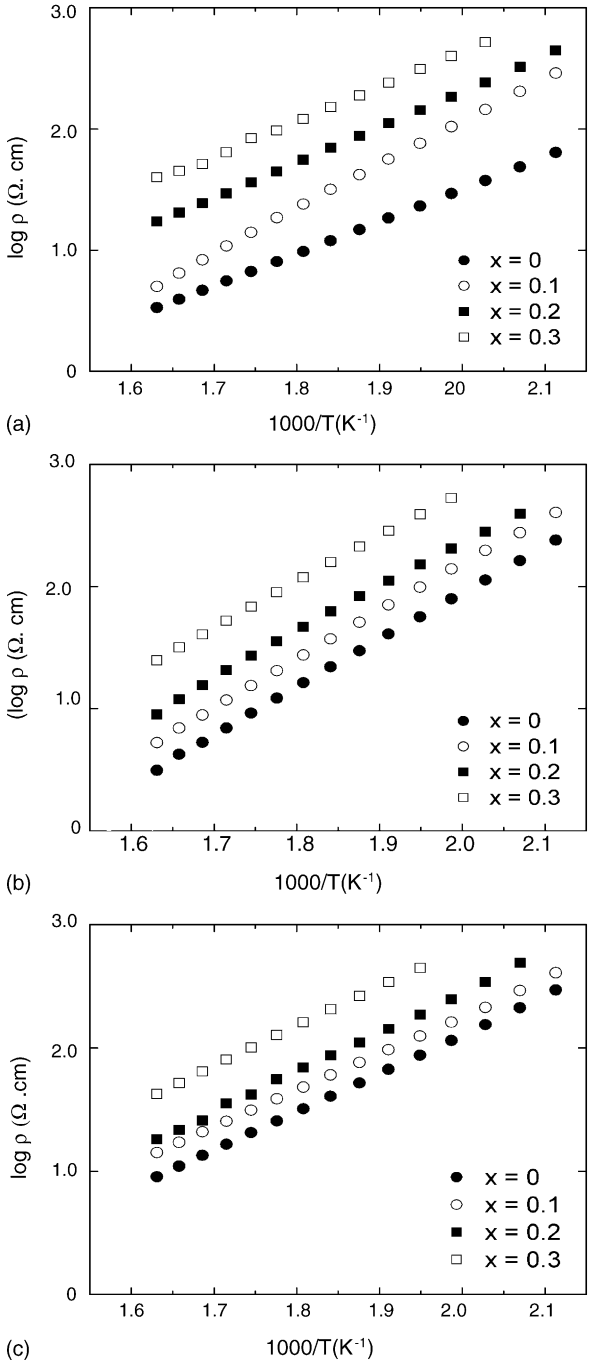

Fig. 5. Plots of $\log \rho$ vs. $1/T$ for the $FeMg_{0.7}Cr_{0.6}Co_{0.7-x}Al_xO_4$ ($x = 0$, 0.1, 0.2, and 0.3) thick film NTC thermistors sintered at (a) 1300 °C, (b) 1350 °C, and (c) 1400 °C.

Table 1
Resistivity at 240 °C, $B_{240/300}$ constant, and activation energy for the $FeMg_{0.7}Cr_{0.6}Co_{0.7-x}Al_xO_4$ ($x = 0$, 0.1, 0.2, and 0.3) thick film NTC thermistors sintered at 1300, 1350, and 1400 °C

Sintering temperature (°C)	Sample	240 °C resistivity (Ω cm)	$B_{240/300}$ constant (K)	Activation energy (eV)
1300	$FeMg_{0.7}Cr_{0.6}Co_{0.7}O_4$	23.2	6106	0.524
	$FeMg_{0.7}Cr_{0.6}Co_{0.6}Al_{0.1}O_4$	76.3	8298	0.712
	$FeMg_{0.7}Cr_{0.6}Co_{0.5}Al_{0.2}O_4$	142.9	6727	0.577
	$FeMg_{0.7}Cr_{0.6}Co_{0.4}Al_{0.3}O_4$	311.2	6426	0.551
1350	$FeMg_{0.7}Cr_{0.6}Co_{0.7}O_4$	56.6	8920	0.765
	$FeMg_{0.7}Cr_{0.6}Co_{0.6}Al_{0.1}O_4$	98.5	9078	0.779
	$FeMg_{0.7}Cr_{0.6}Co_{0.5}Al_{0.2}O_4$	150.5	8401	0.721
	$FeMg_{0.7}Cr_{0.6}Co_{0.4}Al_{0.3}O_4$	389.5	8524	0.731
1400	$FeMg_{0.7}Cr_{0.6}Co_{0.7}O_4$	87.4	7086	0.608
	$FeMg_{0.7}Cr_{0.6}Co_{0.6}Al_{0.1}O_4$	124.9	6784	0.582
	$FeMg_{0.7}Cr_{0.6}Co_{0.5}Al_{0.2}O_4$	186.0	7285	0.625
	$FeMg_{0.7}Cr_{0.6}Co_{0.4}Al_{0.3}O_4$	444.6	7282	0.625

The values of activation energy, q, obtained from the linear portion of Fig. 5 and Eq. (2), are listed in Table 1, together with the $B_{240/300}$ constant, i.e., the thermal sensitivity, and the resistivity at 240 °C (ρ_{240}). The $B_{240/300}$ constant can be calculated by the following equation:[1]

$$B_{240/300} = \frac{\ln(R_{240}/R_{300})}{(1/T_{240}) - (1/T_{300})} \quad (3)$$

where R_{240} and R_{300} are the resistances measured at 240 and 300 °C, respectively. This table indicates that the electrical properties of $FeMg_{0.7}Cr_{0.6}Co_{0.7-x}Al_xO_4$ ($x = 0$, 0.1, 0.2, and 0.3) thick film NTC thermistors strongly depend on the composition and sintering temperature. The $B_{240/300}$ constant is very high, ranging from 6106 to 9078 K, compared to nickel manganites.[7] The $FeMg_{0.7}Cr_{0.6}Co_{0.6}Al_{0.1}O_4$ NTC thermistors sintered at 1350 °C showed the highest $B_{240/300}$ constant (9078 K). Sufficiently high values of the B constant are required for useful applications at high temperatures because they are more sensitive to the variation of temperature, leading to more accurate and smaller variation in temperature measurements. The reason for the dependence of the B constant on the sintering temperature and composition is not still clear at present. To elucidate the detailed nature of the dependence of the B constant, further investigation will be necessary, i.e., exact carrier concentration and mobility, the distribution of cations in spinel structure, and the defect structure of the samples. The calculated activation energies of charge carriers range from 0.524 to 0.779 eV. The high activation energy is probably caused by the random distribution of the differently charged cations at octahedral sites.[26]

The general trend is for the resistivity to significantly increase with increasing both the sintering temperature and the Al_2O_3 content. The main reason for an increase in the resistivity with the sintering temperature is due to an increase in the amount of insulating $MgAl_2O_4$ resulting from the partial decomposition of the solid solutions of Fe–Mg–Cr–Co–(Al) oxides during sintering, as discussed previously. In addition, two possible reasons for the increase in the resistivity with the Al_2O_3 content are as follows: (1) The amount of insulating $MgAl_2O_4$ increased with Al_2O_3 content, increasing the resistivity. (2) Before the introduction of the Al_2O_3 in the thermistors, Co^{2+}/Co^{3+} ions have a preference for octahedral sites according to the crystal field theory,[32] providing a basis for hopping. As the amount of Al_2O_3 in the thermistors increases, that of Co_3O_4 in the thermistors decreases, leading to a decrease in Co^{2+}/Co^{3+} ions on octahedral sites. In order to preserve the overall electrical neutrality of the material, some of the Fe^{3+} on octahedral sites change its valency to Fe^{2+}. This gives rise to a decrease in the amount of Fe^{2+}/Fe^{3+} ions on octahedral sites, which are responsible for hopping and conductivity,[33] resulting in an increase in the resistivity. Electrical conduction occurs via small polaron hopping between Fe^{2+} and Fe^{3+} ions on the octahedral sites. Fig. 6 shows ρ_{240} as a function of the Al_2O_3 content and sintering temperature for the $FeMg_{0.7}Cr_{0.6}Co_{0.7-x}Al_xO_4$ ($x = 0$, 0.1, 0.2, and 0.3) thick film NTC thermistors.

On the basis of the experimental electrical properties for the various $FeMg_{0.7}Cr_{0.6}Co_{0.7-x}Al_xO_4$ ($x = 0$, 0.1, 0.2, and 0.3) thick film NTC thermistors (Table 1), it is apparent that the values of ρ_{240} and the $B_{240/300}$ constant are adjustable to the desired values by changing the Al_2O_3 content and

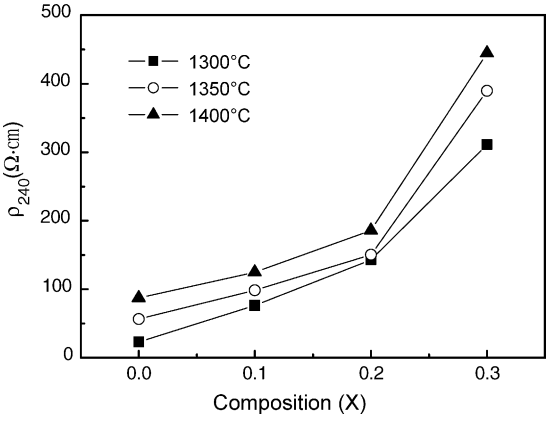

Fig. 6. ρ_{240} as a function of Al_2O_3 content and sintering temperature for $FeMg_{0.7}Cr_{0.6}Co_{0.7-x}Al_xO_4$ ($x = 0$, 0.1, 0.2, and 0.3) thick film NTC thermistors.

the sintering temperature of the NTC thermistors. It is concluded that $FeMg_{0.7}Cr_{0.6}Co_{0.7-x}Al_xO_4$ ($0 \le x \le 0.3$) ceramics are desirable as advanced semiconducting materials for NTC thermistor applications in a wide temperature range.

4. Conclusions

Major phases present in the sintered bodies of $FeMg_{0.7}Cr_{0.6}Co_{0.7-x}Al_xO_4$ ($x = 0$, 0.1, 0.2, and 0.3) thick film NTC thermistors were identified as the solid solutions of the constituent oxides and insulating $MgAl_2O_4$. The $MgAl_2O_4$ was likely to be formed by the partial decomposition of the solid solutions during sintering. The amount of $MgAl_2O_4$ increased with increasing sintering temperature, leading to an increase in the resistivity. A linear relationship between the log resistivity and the reciprocal of the absolute temperature for the prepared $FeMg_{0.7}Cr_{0.6}Co_{0.7-x}Al_xO_4$ ($x = 0$, 0.1, 0.2, and 0.3) thick film NTC thermistors was observed, indicative of an NTC thermistor characteristic. The resistivity significantly increased with increasing both the sintering temperature and Al_2O_3 content. The 240 °C resistivity and the $B_{240/300}$ constant ranged from 23.2 to 444.6 Ω cm and 6106 to 9078 K, respectively, indicating a much higher resistivity and thermal sensitivity, compared to nickel manganites. These results give rise to interesting industrial applications as NTC thermistors over a wide temperature range.

References

1. Macklen, E. D., *Thermistors*. Electrochemical Publications Ltd, Ayr, Scotland, 1979.
2. Csete de Györgyfalva, G. D. C., Nolte, A. N. and Reaney, I. M., Correlation between microstructure and conductance in NTC thermistors produced from oxide powders. *J. Eur. Ceram. Soc.*, 1999, **19**, 857–860.
3. Brabers, V. A. M., Setten, F. M. V. and Knapen, P. S. A., X-Ray photoelectron spectroscopy study of the cation valencies in $NiMn_2O_4$. *J. Solid State Chem.*, 1981, **49**, 93–98.
4. Larson, E. G., Arnott, R. J. and Wickham, D. G., Preparation, semiconduction and low-temperature magnetization of the system $Ni_{1-x}Mn_{2+x}O_4$. *J. Phys. Chem. Solids*, 1962, **23**, 1771–1781.
5. Golestani-Fard, F., Azimi, S. and Mackenzie, K. J. D., Oxygen evolution during the formation and sintering of nickel-manganese oxide spinels for thermistor applications. *J. Mater. Sci.*, 1987, **22**, 2847–2851.
6. Vakiv, M., Shpotyuk, O., Mrooz, O. and Hadzaman, I., Controlled thermistor effect in the system $Cu_xNi_{1-x-y}Co_{2y}Mn_{2-y}O_4$. *J. Eur. Ceram. Soc.*, 2001, **21**, 1783–1785.
7. Park, K., Bang, D. Y., Kim, J. G., Kim, J. Y., Lee, C. H. and Choi, B. H., Influence of the composition and the sintering temperature on the electrical resistivities of Ni-Mn-Co-(Fe) Oxide NTC thermistors. *J. Korean Phys. Soc.*, 2002, **41**, 692–694.
8. Metz, R., Caffin, J. P., Legros, R. and Rousset, A., The preparation, characterization and electrical properties of copper manganite spinels, $Cu_xMn_{3-x}O_4$, $0 \le x \le 1$. *J. Mater. Sci.*, 1989, **24**, 83–87.
9. Kshirsagar, S. T., Electrical and crystallographic studies of the system $Cu_xNi_{1-x}Mn_2O_4$. *J. Phys. Soc. Jpn*, 1969, **27**, 1164–1170.
10. Fu, S. L. and Ho, I. C., The NTCR effect of V_2O_5-doped $(Ba_{0.8}Sr_{0.2})(Ti_{0.9}Zr_{0.1})O_3$ ceramics. *J. Mater. Sci. Lett.*, 1989, **8**(9), 999–1000.
11. Carter, D. C. and Mason, T. O., Electrical properties and site distribution of cations in $(Mn_yCo_{1-y})_{0.4}Fe_{2.6}O_4$. *J. Am. Ceram. Soc.*, 1988, **71**, 213–218.
12. Battault, T., Legros, R. and Rousset, A., Structural and electrical properties of iron manganite spinels in relation with cationic distribution. *J. Eur. Ceram. Soc.*, 1995, **15**, 1141–1147.
13. Macklen, E. D., Electric conductivity and cation distribution in nickel manganite. *J. Phys. Chem. Solids*, 1986, **47**, 1073–1079.
14. Erickson, D. S. and Mason, T. O., Nonstoichiometry, cation distribution, and electrical properties in Fe_3O_4–$CoFe_2O_4$ at high temperature. *J. Solid State Chem.*, 1985, **59**, 42–53.
15. Feltz, A., Töpfer, J. and Schirrmeister, F., Conductivity data and preparation routes for $NiMn_2O_4$ thermistor ceramics. *J. Eur. Ceram. Soc.*, 1992, **9**, 187–191.
16. Dorris, S. E. and Mason, T. O., Electrical properties and cation valencies in Mn_3O_4. *J. Am. Ceram. Soc.*, 1988, **71**, 379–385.
17. Suzuki, M., A.C. hopping conduction in Mn–Co–Ni–Cu complex oxide semiconductors with spinel structure. *J. Phys. Chem. Solids*, 1980, **41**, 1253–1260.
18. Austin, I. G. and Mott, N. F., Polarons in crystalline and noncrystalline materials. *Adv. Phys.*, 1969, **18**, 41–102.
19. Oh, G-Y., Energy spectrum of a triangular lattice in a uniform magnetic field: effect of next-nearest-neighbor hopping. *J. Korean Phys. Soc.*, 2000, **37**(5), 534–539.
20. Brabers, V. A. M. and Terhell, J., Electrical conductivity and cation valencies in nickel manganite. *Phys. State Sol. A*, 1982, **69**, 325–332.
21. Töpfer, J. and Feltz, A., Investigations on electronically conducting oxide systems XXIV[1]: preparation and electrical properties of the spinel series $Cu_zNiMn_{2-z}O_4$. *Solid State Ionics*, 1993, **59**, 249–256.
22. Sarkar, S. K., Sharma, M. L., Bhaskar, H. L. and Nagpal, K. C., Preparation, temperature and composition dependence of some physical and electrical properties of mixtures within the NiO–Mn_3O_4 system. *J. Mater. Sci.*, 1984, **19**, 545–551.
23. Gillot, B., Baudour, J. L., Bouree, F., Metz, R., Legros, R. and Rousset, A., Ionic configuration and cation distribution in cubic nickel manganite spinels $Ni_xMn_{3-x}O_4$ ($0.57 < x < 1$) in relation with thermal histories. *Solid State Ionics*, 1992, **58**, 155–161.
24. Hill, D. C. and Tuller, H. L., In *Ceramic Material for Electronics: Processing, Properties, and Applications*, ed. R. C. Buchanan. Marcel Dekker, New York, 1986. p. 272.
25. Feltz, A., Kriegel, R. and Pölzl, W., $Sr_7Mn_4O_{15}$ ceramics for high temperature NTC thermistors. *J. Mater. Sci. Lett.*, 1999, **18**, 1693–1695.
26. Feltz, A., Perovskite forming ceramics of the system $Sr_xLa_{1-x}Ti^{IV}{}_{x+y}Co^{II}{}_yCo^{III}{}_{1-x-2y}O_3$ for NTC thermistor applications. *J. Eur. Ceram. Soc.*, 2000, **20**, 2367–2376.
27. Sarrion, M. L. M. and Morales, M., Preparation and characterization of NTC thermistors based on $Fe_{2+\delta}Mn_{1-x-\delta}Ni_xO_4$. *J. Mater. Sci.*, 1995, **30**, 2610–2615.
28. Fagan, J. G. and Amarkoon, V. R. W., Reliability and reproducibility of ceramic sensors: part I, NTC thermistors. *Am. Ceram. Soc. Bull.*, 1993, **72**, 70–79.
29. Hasegawa, K., Nishimori, H., Tatsumisago, M. and Minami, T., Effect of polyacrilic acid on the preparation of thick silica films by sol–gel deposition. *J. Mater. Sci.*, 1998, **33**, 1095–1098.
30. Nicholson, P. S., Searcher, P. and Datta, S., Producing ceramic laminate composites by EDP. *Am. Ceram. Soc. Bull.*, 1996, **75**, 48–51.
31. Park, K., Unpublished work.
32. Moulson, A. J. and Herbert, J. M., *Electroceramics*. Chapman & Hall, London, 1993.
33. Yoo, H. I. and Tuller, H. L., Iron-excess manganese ferrite: electrical conductivity and cation distributions. *J. Am. Ceram. Soc.*, 1987, **70**, 388–392.